SAND2013-4865C

Theory and Analysis of Liquid-Oxygen–Hydrogen Interface Dynamics in Liquid Rockets at Supercritical Pressures

Rainer N. Dahms[1] and Joseph C. Oefelein[2]
Combustion Research Facility, Sandia National Laboratories, Livermore, CA 94551, USA

Liquid injection in systems such as liquid rockets where the working fluid exceeds the thermodynamic critical condition of the liquid phase is not well understood. Under some conditions when operating pressures exceed the liquid phase critical pressure, surface tension forces become diminished when the classical low-pressure gas-liquid interface is replaced by a diffusion-dominated mixing layer. Modern theory, however, still lacks a physically-based model to explain the conditions under which this transition occurs. In this paper, we derive a coupled model to obtain a theoretical analysis that quantifies these conditions for general multicomponent liquid injection processes. Our model applies a modified 32-term Benedict-Webb-Rubin equation of state along with corresponding combining and mixing rules that accounts for the relevant thermodynamic non-ideal multicomponent mixture states in the system. This framework is combined with Linear Gradient Theory, which facilitates the calculation of the vapor-liquid molecular structure. Dependent on oxygen and hydrogen injection temperatures, our model shows interfaces with substantially increased thicknesses in comparison to interfaces resulting from lower injection temperatures. Contrary to conventional wisdom, our analysis reveals that LOX-H2 molecular interfaces break down not necessarily because of vanishing surface tension forces, but because of the combination of broadened interfaces and a reduction in mean free molecular path at high pressures. Then, these interfaces enter the continuum length scale regime where, instead of inter-molecular forces, transport processes dominate. Based on this theory, a regime diagram for LOX-H2 mixtures is introduced that quantifies the conditions under which classical sprays transition to dense-fluid jets.

I. Introduction

INJECTION of liquid fuel in systems where the working fluid exceeds the thermodynamic critical pressure of the liquid phase is not well understood. Depending on pressure, injected jets can exhibit two distinctly different sets of evolutionary processes. At low subcritical pressures, the classical situation exists where a well-defined molecular interface separates the injected liquid from ambient gases and causes the presence of surface tension. Interactions between dynamic shear forces and surface tension promote primary atomization, secondary breakup, and evaporation processes. As ambient pressures approach or exceed the critical pressure of the liquid, however, the situation may become quite different. Under these conditions, interfacial diffusion layers can develop, apparently as a consequence of both vanishing surface tension forces and locally diminishing gas-liquid interfaces. The lack of inter-molecular forces and a distinct interfacial structure promotes diffusion dominated mixing processes prior to atomization. As a consequence, injected jets evolve in the presence of exceedingly large but continuous thermo-physical gradients in a manner that is markedly different from the classical assumptions.

Mayer *et al.*,[1,2] were one of the first to show the distinct changes described above. The flow visualization studies conducted by Mayer and Tamura,[2] for example, have illustrated these trends for the case of a LOX–H_2 shear-coaxial injector element. The two extremes are shown in Fig. 1. When LOX and LN2 are injected at low-subcritical pressures, atomization occurs forming a distinct spray as described above. Ligaments are detached from the jet surface forming spherical drops that subsequently breakup and vaporize. As the chamber pressure approaches the thermodynamic critical pressure of the LOX, the number of drops present diminishes.

Research performed since has provided additional insights related to the structure and dynamics of multiphase flows at high pressures. Chehroudi, Talley and Coy[3] performed a wide range of visualizations. Cryogenic liquids at subcritical temperatures were injected into an environment at supercritical temperatures and various pressures ranging from subcritical to supercritical values. Pure nitrogen and oxygen were injected into environments composed of nitrogen, helium, argon and various mixtures of carbon-monoxide and nitrogen. At low subcritical chamber pressures,

[1]Senior Member of Technical Staff, Reacting Flow Research Department, MS 9051, Member AIAA
[2]Distinguished Member of Technical Staff, Reacting Flow Research Department, MS 9051, Associate Fellow AIAA

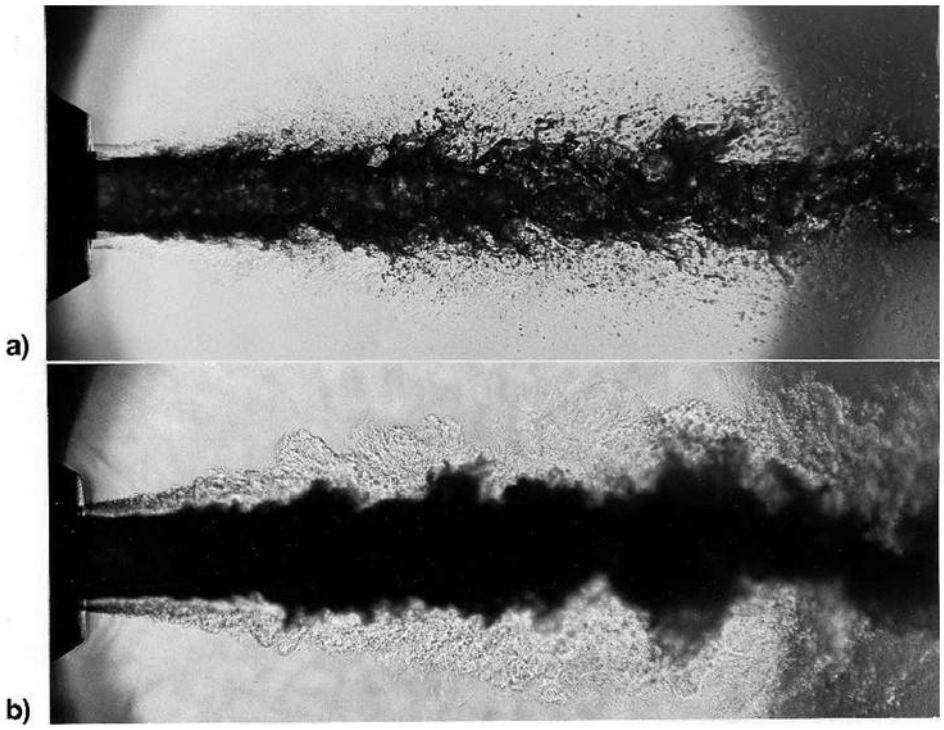

Figure 1. Nonreacting shear-coaxial liquid-nitrogen–helium injector operating at (a) 1.0 *MPa* and (b) 6.0 *MPa*. T_{N2}=97 K, T_{He}=280 K into GHe at T=300 K. From Mayer *et al*[1].

the jets showed surface irregularities that amplified downstream, exhibiting intact, shiny, but wavy surface features that eventually broke up. A further increase of chamber pressure at constant jet initial and ambient temperatures caused the formation of many small drops. As the chamber pressure was further increased, the transition to a full atomization regime was inhibited near but slightly below the critical pressure. The jet structure at this point changed and began to resemble a turbulent gas jet with no detectable drops. The reason was attributed to the reduction of surface tension and enthalpy of vaporization as the critical pressure of the injectant is approached. The initial divergence angle of the jet was measured at the jet exit and compared with the divergence angle of a large number of other mixing layer flows, including atomized liquid sprays, turbulent incompressible gaseous jets, supersonic jets, and incompressible but variable density jets. Chehroudi *et al*.[3] also plotted the divergence angle for the cases described above over four orders of magnitude in the gas-to-liquid density ratio. This was the first time such a plot has been reported over this large a range of density ratios. At and above the critical pressure of the injected liquid, jet growth rate measurements agreed quantitatively with the theory for incompressible but variable density gaseous mixing layers. This provides a quantitative parameter to demonstrate that the similarity between the two flows extends beyond a mere qualitative physical appearance. Finally, as the pressure is reduced to progressively more subcritical values, the spreading rate approaches that measured by others for liquid sprays.

Many other works have served to corroborate these observations.[4–14] The absence of surface tension forces under some high-pressure conditions still poses many fundamental questions. For a pure fluid, basic theory dictates that surface tension forces become diminished when the pressure of the liquid phase exceeds its critical value. For multicomponent liquid injection in modern propulsion and power systems, however, modern theory still lacks a first principle explanation for the observed phenomena. According to fundamental physics, surface tension forces diminish when the temperature of the liquid phase exceeds its critical value. Under many conditions in modern propulsion and power systems, however, this mechanism has to be ruled out as a possible explanation for diminishing surface tension forces. As shown in this paper, the temperature of hot unburnt ambient gases is not sufficient to heat up the gas-liquid interface to its critical temperature. Additionally, elevated pressure alone does also not provide the physical explanation for the obtained observations. In contrast to pure fluids, surface tension forces in multicomponent mixtures do not diminish only because the critical pressure of the liquid or the "mixture critical pressure", as defined by Faeth,[15,16] is exceeded. Experimental evidence of substantial surface tension forces in various binary hydrocarbon/nitrogen mix-

tures at high pressures ($p \gg p_{C,L}$, $p > 400$ bar) is provided in the literature.[17–19]

In this paper, we present some of the first fundamentally based theories to explain and quantify the change in the interfacial dynamics that leads to the transition between non-continuum jump conditions associated with classical two phase flows and continuous diffusion dominated mixing processes widely observed at high pressures. Based on the previous work by Dahms et al.,[20] a comprehensive real-fluid multicomponent thermodynamic model is derived to obtain representative detailed gas-liquid interfacial profiles during the fuel injection process. This theoretical framework is then applied to LOX-H2 mixtures and conditions, representative for liquid rockets. Our analysis shows that, under certain high-pressure conditions, gas-liquid interfacial phenomena are not determined by vapor-liquid equilibrium and the presence of surface tension forces anymore. Instead, the interface enters the continuum length scale regime due to a combination of reduced mean free molecular pathways and broadened interfaces. Based on this fundamental theory, a regime diagram for liquid injection is introduced that quantifies the conditions where this transition can occur, coincidentally, at operating pressures comparable to that of the pure oxygen critical pressure. It also shows the conditions under which classical spray and droplet formation can still occur at liquid-phase supercritical pressures.

II. Model Formulation

The starting point of our model is based on the theoretical-numerical framework developed by Oefelein,[21,22] which provides a generalized treatment of the thermodynamics and transport processes for any arbitrary hydrocarbon mixture at near-critical and supercritical conditions. The thermodynamic and transport property scheme is comprehensive and intricate, thus only a skeletal description can be given here. This framework is combined with real-fluid vapor-liquid equilibrium and Linear Gradient Theory,[23,24] which allows us to reconstruct the gas-liquid interface structure to calculate its surface tension and interface thickness.

A. Thermodynamic and Transport Properties

The extended corresponding states model[25,26] is employed using a Benedict-Webb-Rubin (BWR) equation of state to evaluate the *p-v-T* behavior of the inherent dense multicomponent mixtures. Use of modified BWR equations of state in conjunction with the extended corresponding states principle has been shown to provide consistently accurate results over the widest range of pressures, temperatures and mixture states, especially at saturated conditions. Having established an analytical representation for real mixture *p-v-T* behavior, thermodynamic properties are obtained in two steps. First, respective component properties are combined at a fixed temperature using the extended corresponding states methodology to obtain the mixture state at a given reference pressure. A pressure correction is then applied using departure functions of the form given by Reid *et al*. [27, Chapter 5]. These functions are exact relations derived using Maxwell's relations (see for example VanWylen and Sonntag [28, Chapter 10]) and make full use of the real mixture *p-v-T* path dependencies dictated by the equation of state. Standard state properties are obtained using the databases developed by Gordon and McBride[29] and Kee *et al*.[30] Chemical potentials and fugacity coefficients are obtained in a similar manner. Likewise, viscosity and thermal conductivity are obtained using the extended corresponding states methodologies developed by Ely and Hanley.[31,32] Mass and thermal diffusion coefficients are obtained using the methodologies outlined by Bird *et al*.[33] and Hirschfelder *et al*.[34] in conjunction with the corresponding states methodology of Takahashi.[35]

B. Linear Gradient Theory for Gas-Liquid Interface Structures

Gradient Theory provides a widely accepted methodology to calculate detailed interface structures between gases and liquids.[36,37] Gradient Theory presents a thermo-mechanical model of continuous fluid media and converts statistical mechanics of inhomogeneous fluids into non-linear boundary value problems. At equilibrium, as applied in this paper, the model has been shown in detail to be equivalent to mean-field molecular theories of capillarity. The solid foundations of this theory were established by van der Waals in 1893 and reformulated later by Cahn and Hilliard in 1958. Over past decades, Gradient Theory has been successfully applied to a wide variety of fluids: hydrocarbons and their mixtures, polar compounds and their mixtures, polymer and polymer melts, vapor-liquid and liquid-liquid interfaces. Recently, Gradient Theory has even been successfully compared to Monte Carlo molecular simulations of vapor-liquid and liquid-liquid interfaces.[38–40] There, Gradient Theory proved successful in capturing both surface tension and details of subcritical vapor-liquid molecular interfacial structures. Linear Gradient Theory has been derived

from Gradient Theory by assuming a linearized minimization function of the Helmholtz free energy density distribution across the vapor-liquid interface for the calculation of the interfacial density profiles. Linear Gradient Theory has proven successful in calculating binary and multicomponent interface states of the kind considered here.[23,24]

The interfacial profile of a planar multicomponent gas-liquid interface is obtained by minimizing the Helmholtz free energy, which is expanded as a Taylor series and truncated at lower spatial derivatives according to the following equation[36,37]

$$\sum_i \sum_j \frac{1}{2} \kappa_{ij} \frac{d\rho_{M,i}}{dn} \frac{d\rho_{M,j}}{dn} = \bar{\omega}(\rho_M) - \bar{\omega}_s \tag{1}$$

Here κ_{ij} is the influence parameter, assumed to be density-independent,[41] with ρ_M as the molar density, n as the normal interface direction and $\bar{\omega}_s = -p_s$ as the equilibrium pressure. The grand thermodynamic potential energy density is defined as

$$\bar{\omega}(\rho_M) = f_0(\rho_M) - \sum_i \rho_{M,i} \mu_i \tag{2}$$

with f_0 as the Helmholtz free energy density of the homogeneous fluid and μ_i as the chemical potential. Using Gradient Theory, the surface tension σ and spatial interface dimension z can then be calculated once the species density profiles within the interface are known:

$$\sigma = \int_{\rho_{I,V}}^{\rho_{I,L}} \sqrt{2\kappa(\bar{\omega}(\rho_M) - \bar{\omega}_s)} d\rho_I \tag{3}$$

and

$$z = z_0 + \int_{\rho_{I,0}}^{\rho_I} \sqrt{\frac{\kappa}{2(\bar{\omega}(\rho_M) - \bar{\omega}_s)}} d\rho_I \tag{4}$$

with subscripts I as the reference component (fuel) and with the mixture influence parameter κ calculated following

$$\kappa = \sum_i \sum_j \kappa_{ij} \frac{d\rho_i}{d\rho_I} \frac{d\rho_j}{d\rho_I} \quad . \tag{5}$$

The term κ_{ij} results from the pure component influence parameter calculated according to Lin et al.[36] The boundary conditions of the bulk vapor and liquid phases, referred to by indices V and L in Eq.(3), are obtained from real-fluid multicomponent vapor-liquid equilibrium calculations. In Gradient Theory, the species density profiles in the reference space ρ_I of Eqs.(3) and (4) are obtained from non-linear equations, derived from Eq.(1). They prescribe the species density change with respect to the reference (fuel) component. In contrast to Gradient Theory, Linear Gradient Theory applies linear equations. Then, the characteristic interface thickness ℓ_{VLE} is calculated following the criterion from Lekner and Henderson[42]

$$\ell_{\text{VLE}} = \int_{\rho_{I,0.1}}^{\rho_{I,0.9}} \sqrt{\frac{\sum_i \sum_j \kappa_{ij} \frac{d\rho_i}{d\rho_I} \frac{d\rho_j}{d\rho_I}}{2\left(f_0(\rho_M) - \sum_i \rho_{M,i}\mu_i - \bar{\omega}_s\right)}} d\rho_I \tag{6}$$

$$\tag{7}$$

III. Results and Discussion

To obtain a comprehensive analysis of the liquid injection process, the mixture fraction variable is introduced as $Z = {}^{m_1}/_{(m_1+m_2)}$, with m_1 as the hydrogen fuel (H_2) stream mass and m_2 as the oxidizer (LOX) stream mass, respectively.

Results of real-fluid multicomponent vapor-liquid equilibrium (VLE) calculations, obtained using the 32-term BWR mixture state equation, are shown in Fig. 2. Corresponding thermodynamic equilibrium conditions read:

$$\begin{aligned} T^V &= T^L \\ p^V &= p^L \\ \mu_i^V &= \mu_i^L \end{aligned} \tag{8}$$

with T as the temperature, p as the pressure, and μ_i as the chemical potential of species i. Figure 2 shows vapor liquid equilibrium compositions for the LOX-H2 binary system at different chamber pressures. The calculations show

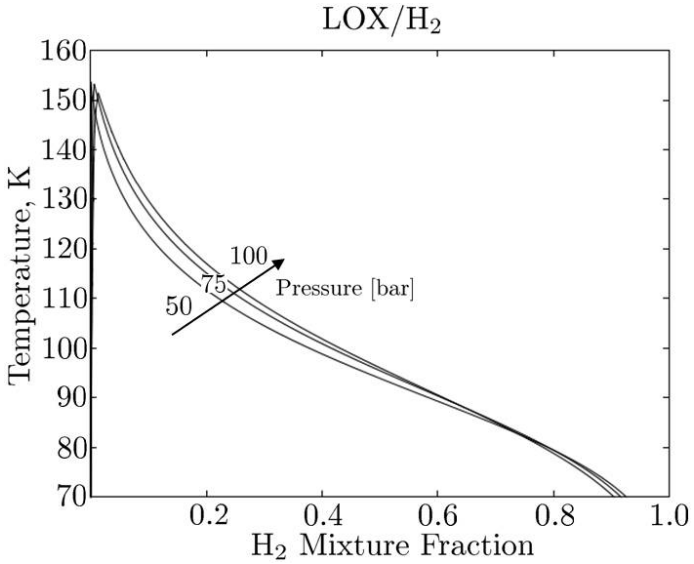

Figure 2. Temperature and mixture composition conditions at various pressures using real-fluid LOX-H2 vapor liquid equilibrium calculations.

that the critical temperature, above which vapor-liquid equilibrium cannot exist anymore, decreases with increasing pressure due to an increase of dissolved hydrogen into the liquid phase. As shown in Fig. 3, this decrease in critical temperature scales linearly with pressure. After having established a framework to compute two-phase states, the envelope of single-phase conditions is calculated using adiabatic mixing temperatures.

Such temperatures are computed assuming an enthalpy distribution linear in mixture fraction space. The modified 32-term BWR equation of state is then applied to calculate the temperature for each composition determined by the mixture fraction in order to match the prescribed linear enthalpy distribution. In Fig. 4, the adiabatic mixture temperature is presented for a constant chamber pressure of p=60 bar and liquid oxygen and gaseous hydrogen coaxial injection temperatures of T_{LOX}=100 K and T_{GH2}=300 K, respectively. This temperature distribution is combined with prior calculations of vapor-liquid equilibrium. The chamber pressure defines the envelope of temperature/mixture conditions under which a vapor-liquid equilibrium is possible. Likewise, the adiabatic mixing temperatures define the envelope of representative temperature conditions under which a vapor state (if it exists), which mixes with the ambient gas, is possible. Therefore, the representative interface state is found at the

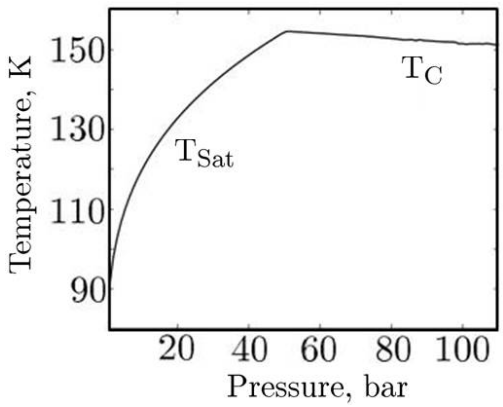

Figure 3. Saturation and critical mixture temperature of oxygen-hydrogen mixtures at various pressures.

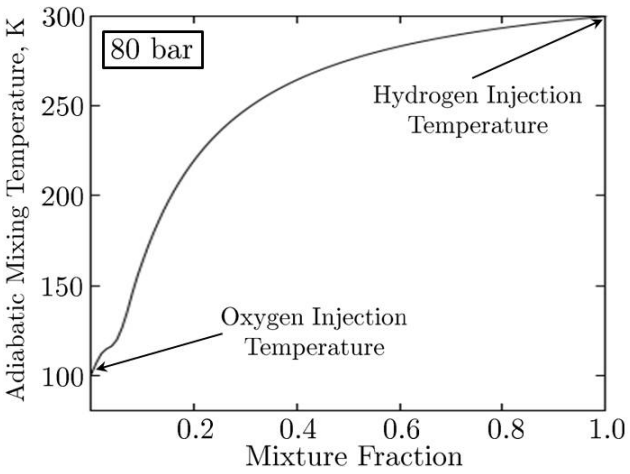

Figure 4. Adiabatic mixing temperature for a LOX-H2 systems at p=80 bar.

temperature intersection points between adiabatic mixing and vapor equilibrium state temperatures as shown in Fig. 5. The pressure of the interface is assumed to be equal to the chamber pressure. This analysis suggests a saturated mixture condition at a temperature of T≈133 K. The analysis also shows that the temperature of the unburnt ambient mixture is not sufficient to heat up the temperature of the liquid to its critical value. A required mixing line to actually obtain such critical conditions is also illustrated in Fig. 5 which shows its nonphysical nature. This result implies the existence of a distinct two-phase interface with surface tension forces for almost all operating conditions when the liquid is injected at subcritical temperatures. This, however, appears to be in conflict with experimental evidence of vanishing two-phase interfaces at such conditions.[1] Vapor-liquid equilibrium calculations do provide the compositions and mixture states of the respective vapor and liquid phases at given temperature and pressure conditions. However,

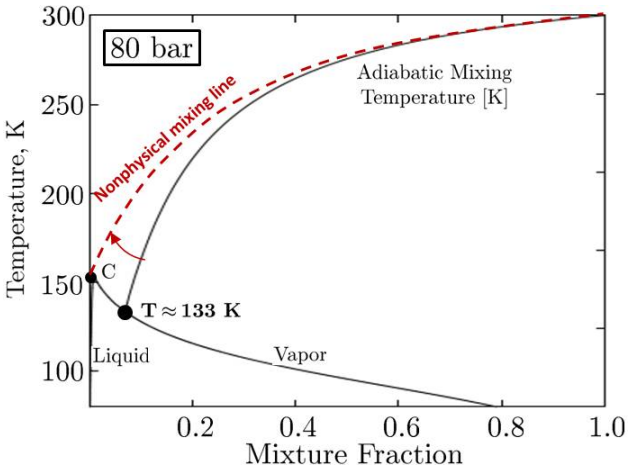

Figure 5. Representative two-phase interface state for a LOX-H2 systems at p=80 bar obtained from the temperature intersection point between adiabatic mixing and vapor-liquid equilibrium temperatures. The adiabatic mixing temperature cannot heat up the liquid to its critical temperature.

such calculations do not provide information about the spatial distribution of these compositions or the value of surface tension. Therefore, Linear Gradient Theory is applied to reconstruct the detailed density profile and the strength of surface tension forces. The equilibrium phase states provide the boundary conditions for the interfacial profile calculation. Figure 6 presents the calculated vapor-liquid interfacial mixture density profiles for two interface states using Linear Gradient Theory. At the high-temperature condition, the interface shows substantially reduced values of density differences between vapor and liquid states and is distinctively thicker than at the corresponding lower temperature condition. The relevance of this thickness for interface phenomena is highlighted by comparing it to the

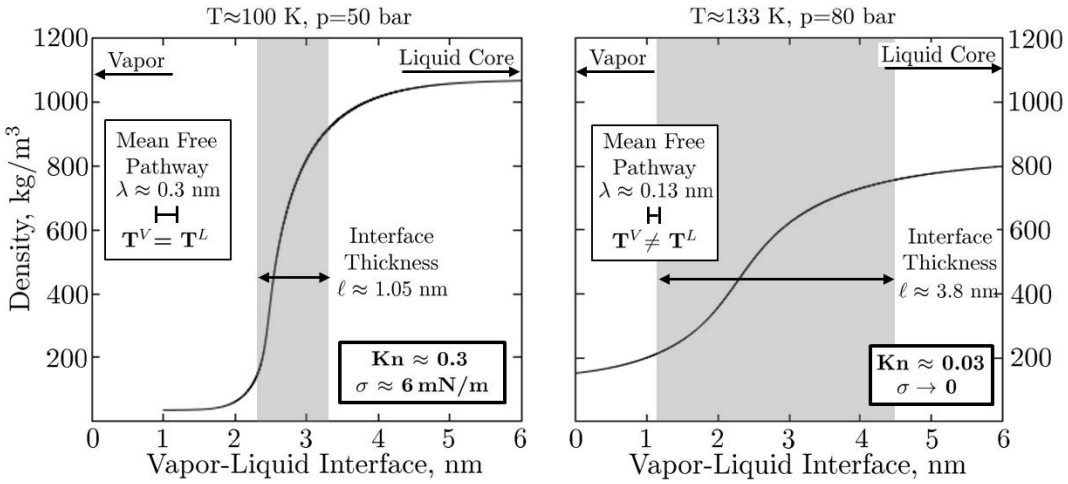

Figure 6. Density profiles across vapor-liquid interfaces computed from Linear Gradient Theory.

mean free pathway, also shown in Fig. 6 for reference. Fluid particles equilibrate over distances comparable to the molecular length scales, represented by such mean free pathways. As the mean free pathway at the low-temperature interface is comparable to the interface thickness, the temperature of the vapor equilibrates with the temperature of the liquid (T^V=T^L) and their interfacial processes are governed by molecular dynamics, thereby justifying the applied vapor-liquid equilibrium assumptions. This interface exhibits surface tension forces, supports evaporation and heat of vaporization phenomena, and is therefore expected to lead to the classical spray phenomena as two-phase theory applies. At the high-temperature interface, however, the situation is reversed. The mean free pathway has become more than an order of magnitude shorter than the interface thickness. Then, vapor-liquid interfacial processes are not governed by molecular dynamics anymore as this interface enters the continuum regime. Under the conditions here, the heat flux across the interface becomes linearly related to the temperature gradient. As the ambient gas temperature is substantially higher than the liquid temperature, the temperature equilibrium assumption between vapor and liquid, compare Eq. (8), also breaks down ($T^V \neq T^L$). Vapor-liquid equilibrium assumptions and classical two-phase theory do not apply. The calculated vapor-liquid equilibrium value of surface tension forces therefore diminishes as the thickness of this interface substantially increases. Such interfaces cannot support atomization and evaporation phenomena. These two distinctively different two-phase interfacial phenomena are classified using a Knudsen-number criterion:

$$\mathrm{Kn} = \frac{\lambda}{\ell} < 0.1 \rightarrow \text{Continuum Regime} \tag{9}$$

with λ as the representative mean free pathway of the interface. It is calculated at the corresponding vapor equilibrium condition as the most conservative mixture state within the interface. Assuming the validity of ideal gas laws, the mean free pathway λ, conditioned on the vapor state x'', reads

$$< \lambda | x'' >= \frac{k_B T}{\sqrt{2}\pi p d^2} \tag{10}$$

with k_B as the Boltzmann constant, T as the interface temperature, p as the interface pressure, and d as the hard sphere diameter of the average molecule. The average molecule size is calculated as

$$d = \sum_i X_i d_i \tag{11}$$

with X_i as the species mole fractions provided by the vapor equilibrium composition and d_i as the respective molecular size of each species. The vapor-liquid equilibrium interface thickness ℓ is calculated from Eq. (6). Knudsen numbers less than $\mathrm{Kn} < 0.1$ characterize interfaces which will enter the continuum regime governed by the Navier-Stokes equations. Knudsen numbers greater than $\mathrm{Kn} > 0.1$ characterize non-continuum flows. As shown in Fig. 6, this Knudsen number criterion confirms for the low-temperature interface state ($\mathrm{Kn} \approx 0.3 > 0.1$) that classical two-phase theory applies, while the same criterion for the high-temperature interface

shows (Kn $\approx 0.03 < 0.1$), that continuum assumptions including the definition of the mixture fraction become valid across the interface. The significance of the temperature in the broadening of vapor-liquid interfaces is shown in Figure 7. The analysis shows that the interface thickness increases exponentially with temperature. Surface tension forces, on the other hand, are known to decrease only linearly with temperature.

The high-temperature case, where the continuum fluid mechanic assumptions have been shown to apply across the whole mixture fraction space, is further analyzed. The envelope of thermodynamic mixture state conditions during the fuel injection process is considered by extending the classical P-V-T phase diagram of pure components to a 4D pressure-temperature-density-mixture fraction (P-T-ρ-Z) phase diagram of oxidizer and fuel streams. As a homogeneous phase property model, the equation of state computes pseudo-pure fluid vapor-liquid phase transitions without a composition change ($x' = x''$; x': Liquid mole fraction; x'': Vapor mole fraction). The resulting pseudo-pure saturation points are processed for each mixture state Z and are shown in Fig. 8. This allows the definition of the critical line of the mixture as the envelope of critical temperatures $T = T_{Crit}(Z)$ and critical pressures $p = p_{Crit}(Z)$ for each mixture state Z. These properties are calculated using the 32-term BWR mixture state equation using the theory of extended corresponding states. The implicitly applied pseudo-pure fluid model assumption $x' = x''$ is fulfilled at the critical point of a multicomponent mixture. Then, the thermodynamic regimes of liquid, compressed liquid, vapor, ideal gas, and the supercritical state can be defined as shown in Fig. 8. The critical pressure of the mix-

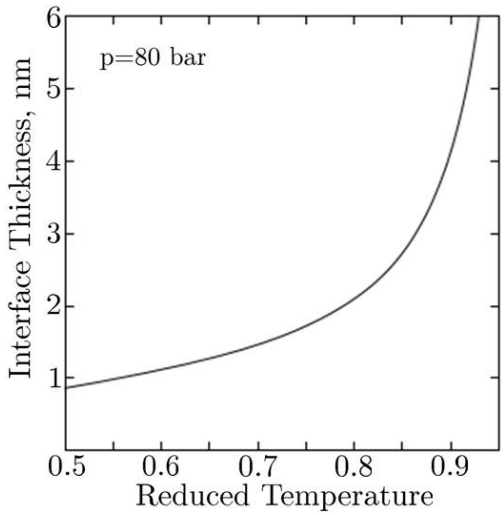

Figure 7. LOX-H2 interface thickness of as a function of the reduced temperature.

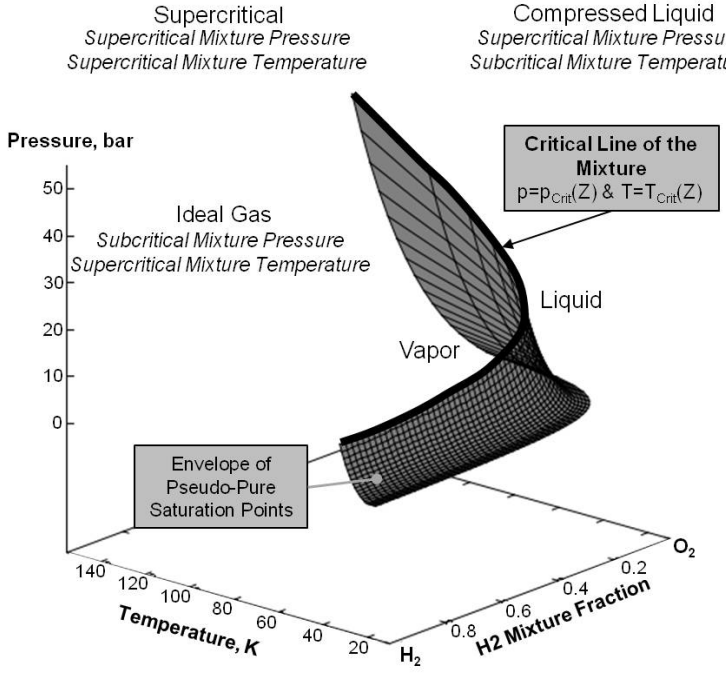

Figure 8. Visualization of the homogeneous-fluid saturation surface in PTZ space of a LOX-H2 system using the theory of extended corresponding states. Then, the critical line of the mixture can be defined as the envelope of pressures and temperatures, critical for each mixture state.

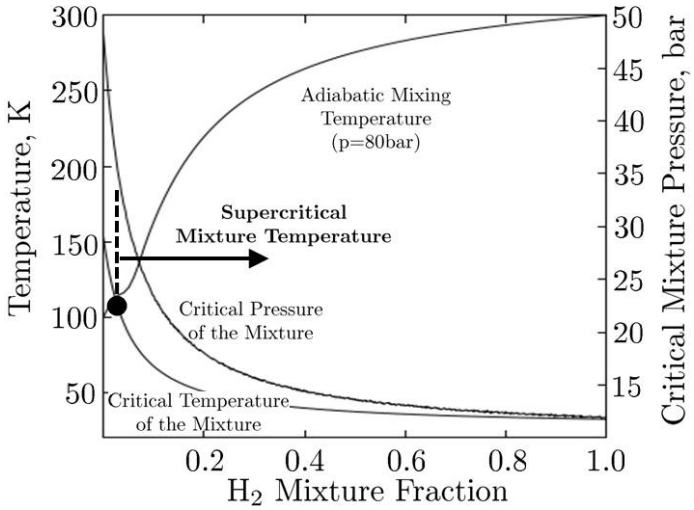

Figure 9. Critical temperature of the mixture $T_{Crit}(Z)$, adiabatic mixing temperature T and critical pressure of the mixture $p_{Crit}(Z)$ as a function of mixture fraction.

ture $p_{Crit}(Z)$ and critical temperature of the mixture $T_{Crit}(Z)$ are presented in Fig. 9, showing that the critical point of each mixture state is determined by non-linear combinations of the pure component critical properties. The adiabatic mixing temperature, already defined in Fig. 4, exceeds the critical temperature for all mixture states $Z \geq Z^{\star} \approx 0.022$.

Informed by this analysis, a thermodynamic mixture state regime diagram is defined and used to analyze the envelope of the liquid injection mixture preparation process, as shown in Fig. 10. The reduced critical pressure of the mixture $p_{Chamber}/p_{Crit}(Z)$ as a function of the mixture fraction variable is shown. The constant chamber pressure is denoted by $p_{Chamber} = 80$ bar and the critical pressure of the mixture, taken from Fig. 9, is denoted by $p_{Crit}(Z)$, respectively. Supercritical mixture pressures are then defined as $p_{Chamber}/p_{Crit}(Z) > 1.0$. Supercritical mixture temperatures are found for mixture states above $Z^{\star} \approx 0.022$, compare Fig. 9. Under the conditions here, the mixture preparation process consists of a continuous phase transition from liquid to gaseous states as the mixing pathway does only cross the compressed liquid and supercritical, but not the two-phase regime. Compressibility factors are also presented for all

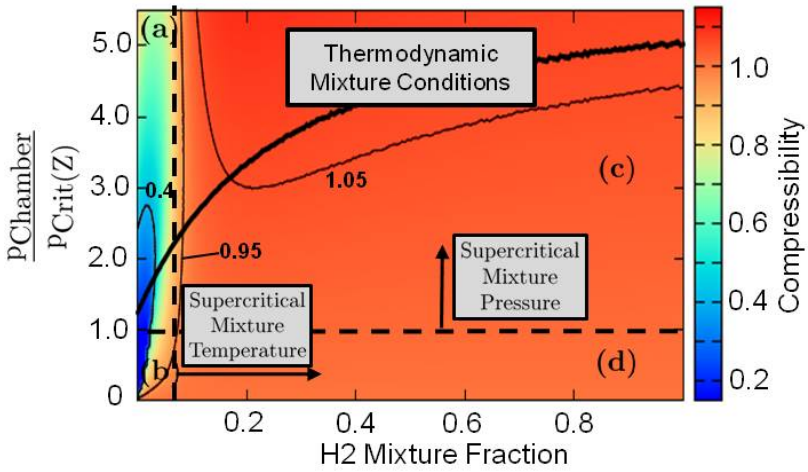

Figure 10. Resultant envelope of thermodynamic mixture state conditions for LOX (T=100 K) and coaxial H2 (T=300 K) injection. The constant chamber pressure ($p = 80$ bar) exceeds the critical pressure p_{Crit}, shown in Fig. 6, for all mixture states. For mixtures above $Z^{\star} \approx 0.022$, the adiabatic mixing temperature exceeds the critical temperature of the mixture. Then, the regimes of compressed liquid (a), mixture saturation (b), supercritical state (c), and ideal gas (d) can be defined.

regime conditions. They emphasize the relevance of the real-fluid property model for mixtures $Z < 0.06$ and validate

the ideal-gas mean free path calculation and the Knudsen-number criterion, defined in Eqs.(10) and (9), respectively, which have been applied for the high-temperature interface vapor state at $Z \approx 0.07 > 0.06$, compare Fig. 5, where this ideal-gas assumption is valid.

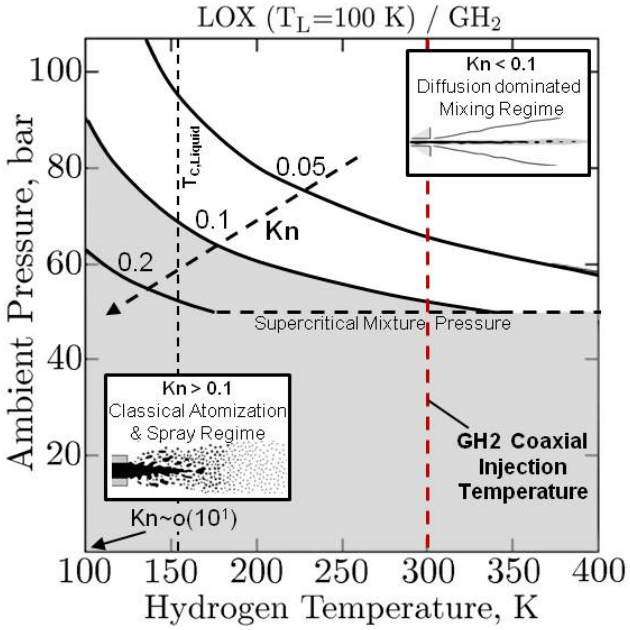

Figure 11. Liquid injection regime diagram for a LOX-H2 system. The oxidizer is injected at T=100 K.

Based on this analysis, a liquid injection regime diagram, which quantifies the conditions under which surface tension forces diminish in multicomponent mixtures, can be defined and is presented in Fig. 11. Regimes of classical sprays (highlighted in grey) and diffusion dominated mixing due to diminished vapor-liquid interfaces are found based on the Knudsen-number criterion, defined in Eq. (9). Figure 11 presents the regime diagram for liquid oxygen injected at a temperature of T_{LOX}=100 K into gaseous hydrogen at varying ambient pressures and temperatures. For a hydrogen coaxial injection temperature of T=300 K, the liquid injection regime diagram suggests that classical spray phenomena do not occur, consistent with experimental observations,[2] at system pressures above the critical pressure of pure oxygen. Instead, the oxygen is injected as a continuous liquid jet with diminished surface tension forces. Then, interfacial convection-diffusion layers develop between the injected liquid and the ambient gas. Such layers are largely affected by non-ideal thermal and transport processes and cannot support evaporation phenomena or the formation of liquid ligaments or droplets. The regime diagram also suggests that, under low-temperature coaxial injection hydrogen temperature, classical spray and droplet formation can still occur at liquid-phase supercritical pressures.

IV. Summary and Conclusions

Past works have suggested that two extremes exist with regard to liquid injection in high-pressure systems. At lower pressures, typically subcritical with respect to the liquid phase, the classical situation exists where a well defined interface separates the injected liquid from ambient gases and causes the presence of surface tension. Under these conditions, surface tension forces form a discontinuous (non-continuum) interface that promotes primary atomization, secondary breakup and the resultant spray phenomena that have been well recognized and is widely assumed. At high-pressure conditions, the situation can become quite different. Under some conditions, a distinct gas-liquid interface may not exist. Instead, injected jets undergo a continuous change of state. Effects of surface tension become diminished and the lack of these inter-molecular forces minimizes or eliminates the formation of drops and promote diffusion dominated mixing processes prior to atomization. Injected jets at such conditions have been observed to evolve in the presence of exceedingly large (but continuous) thermophysical gradients, with no drops present in the flow. In this paper, we have presented a theoretical analysis that explains and quantifies the change in the interfa-

cial dynamics that leads to the transition between the classical non-continuum "jump" conditions associated with two phase flows and the continuous gas-liquid interfacial diffusion layers.

We developed a real-fluid model, that accounts for multicomponent vapor-liquid equilibrium, the presence of surface tension, and the interface states for the two investigated chamber conditions. Within this framework, Linear Gradient Theory was applied to reconstruct the detailed interface structure. The interface resulting from high-temperature hydrogen injection showed a substantially wider interface thickness compared to the low-temperature hydrogen interface. An applied Knudsen-number criterion then revealed a major finding. Contrary to conventional wisdom, continuous gas-liquid interfacial diffusion layers develop not necessarily because of vanishing surface tension forces, but because of the combination of a reduction in mean free molecular path and broadening interfaces, which then enter the continuum length scale regime. Thus, independent of any residual surface tension forces that might be present, the Navier-Stokes equations apply across the high-temperature vapor-liquid interface if the viscous stress term is modified appropriately. Similarly, Fick's diffusion law applies across the vapor-liquid interface resulting in a continuous phase transition during the mixture preparation process.

Based on this finding, the resulting diffusion pathway was studied by developing a thermodynamic regime diagram in mixture fraction space. The envelope of this pathway showed a continuous phase transition from compressed-liquid to gaseous states. Therefore, under the conditions here, subcritical phenomena like primary and secondary breakup processes and evaporation are found not to substantially affect the mixture preparation process. Instead, a dense-fluid-approximation that accounts for the substantial thermodynamic non-idealities and transport anomalies during the liquid injection process is required.

Acknowledgements

The U.S. Department of Energy, Office of Basic Energy Sciences, Division of Chemical Sciences, Geosciences, and Biosciences supported this work. This research was performed at the Combustion Research Facility, Sandia National Laboratories, Livermore, California. Sandia National Laboratories is a multiprogram laboratory operated by Sandia Corporation, a Lockheed Martin Company, for the United States Department of Energy under contract DE-AC04-94-AL85000.

References

[1] W. Mayer, A. Schik, B. Vieille, C. Chaveau, I. Gökalp, D. Talley, and R. Woodward. "Atomization and Breakup of Cryogenic Propellants Under High-Pressure Subcritical and Supercritical Conditions," Journal of Propulsion and Power **14**, 835 (1998).

[2] W. Mayer and H. Tamura. "Propellant Injection in a Liquid Oxygen/Gaseous Hydrogen Rocket Engine," Journal of Propulsion and Power **12**, 1137 (1996).

[3] B. Chehroudi, D. Talley, and E. Coy. "Visual Characteristics and Initial Growth Rates of Round Crygenic Jets at Subcritical and Supercritical Pressures," Phys. Fluids **14**, 850 (2002).

[4] M. Oschwald, J. Smith, R. Branam, J. Hussong, A. Schik, B. Chehroudi, and D. Talley. "Injection of Fluids into Supercritical Environments," Combust. Sci. Tech. **178**, 49 (2006).

[5] M. Habiballah, M. Orain, F. Grisch, L. Vingert, and P. Gicquel. "Experimental Studies of High-Pressure Cryogenic Flames on the Mascotte Facility," Combust. Sci. Tech. **178**, 101 (2006).

[6] K.-C. Lin, S. Cox-Stouffer, and T. Jackson. "Structures and Phase Transition Processes of Supercritical Methane/Ethylene Mixtures Injected into a Subcritical Environment," Combust. Sci. Tech. **178**, 129 (2006).

[7] S. Candel, M. Juniper, G. Singla, P. Scouflaire, and C. Rolon. "Structure and Dynamics of Cryogenic Flames at Supercritical Pressure," Combust. Sci. Tech. **178**, 161 (2006).

[8] N. Zong and V. Yang. "Cryogenic Fluid Jets and Mixing Layers in Transcritical and Supercritcal Environments," Combust. Sci. Tech. **178**, 193 (2006).

[9] J. C. Oefelein. "Mixing and Combustion of Cryogenic Oxygen-Hydrogen Shear-Coaxial Jet Flames at Supercritical Pressure," Combust. Sci. Tech. **178**, 229 (2006).

[10] J. Bellan. "Theory, Modeling and Analysis of Turbulent Supercritical Mixing," Combust. Sci. Tech. **178**, 253 (2006).

[11] L. C. Selle, N. A. Okong'o, J. Bellan, and K. G. Harstad. "Modelling of Subgrid-Scale Phenomena in Supercritical Transitional Mixing Layers: An A Priori Study," J. Fluid Mech. **593**, 57 (2007).

[12] G. Ribert, N. Zong, V. Yang, L. Pons, N. Darabiha, and S. Candel. "Counterflow Diffusion Flames of General Fluids: Oxygen/Hydrogen Mixtures," Combust. Flame **154**, 319 (2008).

[13] L. Pons, N. Darabiha, S. Candel, G. Ribert, and V. Yang. "Mass Transfer and Combustion in Transcritical Non-premixed Counterflows," Combust. Theory Modelling **13**, 57 (2009).

[14] T. Schmitt, Y. Méry, M. Boileau, and S. Candel. "Large-Eddy Simulation of Oxygen/Methane Flames under Transcritical Conditions," Proc. Combust. Inst. **33**, 1383 (2011).

[15] G.M. Faeth, D.P. Dominicis, J.F. Tulpinsky, and D.R. Olson. "Supercritical Bipropellant Droplet Combustion," Proc. Combust. Inst. **12**, 9 (1969).

[16] R.S. Lazar and G.M. Faeth. "Bipropellant Droplet Combustion in the Vicinity of the Critical Point," Proc. Combust. Inst. **13**, 801 (1971).

[17] O.G. Nino-Amezquita, S. Enders, P.T. Jaeger, and R. Eggers. "Measurement and Prediction of Interfacial Tension of Binary Mixtures," Ind. Eng. Chem. Res. **49**, 592 (2010).

[18] J. Dechoz and C. Roze. "Surface Tension Measurement of Fuels and Alkanes at High Pressure Under Different Atmospheres," Appl. Surf. Sci. **229**, 175 (2004).

[19] S. Liu, D. Fu, and J. Lu. "Investigation of Bulk and Interfacial Properties for Nitrogen and Light Hydrocarbon Binary Mixtures by Perturbed-Chain Statistical Associating Fluid Theory Combined with Density-Gradient Theory," Ind. Eng. Chem. Res. **48**, 10734 (2009).

[20] R.N. Dahms, J. Manin, L.M. Pickett, and J.C. Oefelein. "Understanding High-Pressure Gas-Liquid Interface Phenomena in Diesel Engines," Proc. Combust. Inst. **34**, 1667 (2013).

[21] J.C. Oefelein. "Large Eddy Simulation of Turbulent Combustion Processes in Propulsion and Power Systems," Progress in Aerospace Sciences **42**, 2 (2006).

[22] J.C. Oefelein. "Simulation and Analysis of Turbulent Multiphase Combustion Processes at High Pressures," Ph.D. thesis, The Pennsylvania State University, 1997.

[23] Y.-X. Zuo and E.H. Stenby. "A Linear Gradient Theory Model for Calculating Interfacial Tensions of Mixtures," J. Colloid Interface Sci. **182**, 126 (1996).

[24] K.A.G. Schmidt, G.K. Folas, and B. Kvamme. "Calculation of the Interfacial Tension of Methane-Water System with the Linear Gradient Theory," Fluid Phase Equil. **261**, 230 (2007).

[25] T.W. Leland and P.S. Chappelear. "The Corresponding States Principle. A Review of Current Theory and Practice," Industrial and Engineering Chemistry Fundamentals **60**, 15 (1968).

[26] J.S. Rowlinson and I.D. Watson. "The Prediction of the Thermodynamic Properties of Fluids and Fluid Mixtures–I. The Principle of Corresponding States and Its Extensions," Chem. Eng. Sci. **24**, 1565 (1969).

[27] R.C. Reid, J.M. Prausnitz, and B.E. Polling. *The Properties of Liquids and Gases* (McGraw-Hill, New York, 1987).

[28] G.J. VanWylen and R.E. Sonntag. *Fundamentals of Classical Thermodynamics* (John Wiley and Sons, Incorporated, New York, 1986).

[29] S. Gordon and B.J. McBride. "Computer Program for Calculation of Complex Chemical Equilibrium Compositions, Rocket Performance, Incident and Reflected Shocks and Chapman-Jouguet Detonations," NASA SF-273 (1971). Technical report.

[30] R.J. Kee, F.M. Rupley, and J.A. Miller. "Chemkin Thermodynamic Data Base," SAND87-8215B (1990). Technical report.

[31] J.F. Ely and H.J.M. Hanley. "Prediction of Transport Properties. 1. Viscosity of Fluids and Mixtures," Industrial and Engineering Chemistry Fundamentals **20**, 323 (1981).

[32] J.F. Ely and H.J.M. Hanley. "Prediction of Transport Properties. 2. Thermal Conductivity of Pure Fluids and Mixtures," Industrial and Engineering Chemistry Fundamentals **22**, 90 (1981).

[33] R.B. Bird, W.E. Stewart, and E.N. Lightfoot. *Transport Phenomena* (John Wiley and Sons, Incorporated, New York, 1960).

[34] J.O. Hirschfelder, C. F. Curtiss, and R. B. Bird. *Molecular Theory of Gases and Liquids* (John Wiley and Sons, Incorporated, New York, 1964).

[35] S. Takahashi. "Preparation of a Generalized Chart for the Diffusion Coefficients of Gases at High Pressures," Journal of Chemical Engineering of Japan **7**, 417 (1974).

[36] H. Lin, Y.-Y. Duan, and Q. Min. "Gradient Theory Modeling of Surface Tension for Pure Fluids and Binary Mixtures," Fluid Phase Equil. **254**, 75 (2007).

[37] C. Miqueu, B. Mendiboure, and J. Lachaise. "Modeling of the Surface Tension of Multicomponent Mixtures with the Gradient Theory of Fluid Interfaces," Ind. Eng. Chem. Res. **44**, 3321 (2005).

[38] E.A. Müller and A. Mejia. "Interfacial Properties of Selected Binary Mixtures Containing N-Alkanes," Fluid Phase Equil. **282**, 68 (2009).

[39] A. Mejia, J.C. Pamies, D. Duque, H. Seguara, and L.F. Vega. "Phase and Interface Behaviors and Type-I and Type-V Lennard-Jones Mixtures: Theory and Simulations," J. Chem. Phys. **123**, 1 (2005).

[40] C. Miqueu, J.M. Miguez, M.M. Pineiro, T. Lafitte, and B. Mendiboure. "Simultaneous Application of the Gradient Theory and Monte Carlo Molecular Simulation for the Investigation of Methane/Water Interfacial Properties," J. Phys. Chem. B **115**, 9618 (2011).

[41] B.F. McCoy and H.T. Davis. "On the Free Energy Theory of Inhomogeneous Fluids," Phys. Rev. **20**, 1201 (1978).

[42] J. Lekner and J.R. Henderson. "Theoretical Determination of the Thickness of a Liquid-Vapour Interface," Physica A **94**, 545 (1978).